The Effects of Tooth Winding Usage

Karel Hruska[1)] and Martin Sokol[2)]
[1)] University of West Bohemia/Faculty of Electrical Engineering/RICE,
Pilsen, Czech Republic, e-mail: *khruska@kev.zcu.cz*
[2)] University of West Bohemia/Faculty of Electrical Engineering,
Pilsen, Czech Republic, e-mail: *msokol@students.zcu.cz*

Abstract — **The article deals with tooth windings used for permanent magnet machinery, their analyses and after-effects of their usage. The article discusses basic tooth winding properties, possibilities of examination of generated magnetic field and it studies the impact on the machine characteristics. A case study of a designed traction machine equipped with the tooth winding is presented for the purpose of result comparison.**

Keywords — Differential leakage flux, Görges pattern, magnetomotive force, tooth winding, torque, winding factor

I. Introduction

The tooth windings are specific types of multiple-phase concentrated windings widely used for permanent magnet machinery. In comparison to traditional distributed windings they have very reduced winding overhangs, which results in decrease of resistive losses and increase of machine efficiency. This effect is ensured using shortest possible winding step y_{1s} (expressed as amount of slots) equal to one.

The winding step of tooth winding has, opposing to traditional distributed windings, no relation to machine pole pitch and in most cases the winding step is much shorter than machine pole pitch t_p. The result is lowering of the machine winding factor, in many cases even below $k_w = 0.9$, as mentioned in many other papers and publications [1, 2].

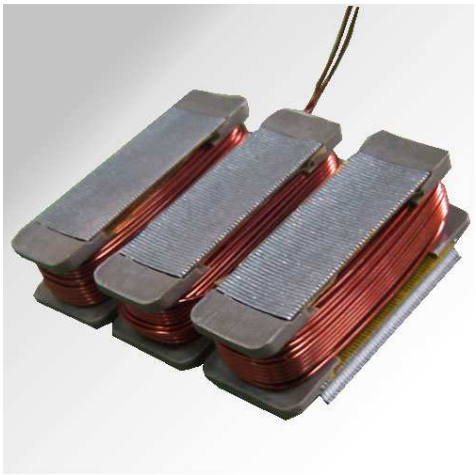

Fig. 1. Tooth winding coils wound on stator segments [3]

A suitable parameter used for description of the tooth windings is the amount of slots per pole and phase q, which is a number unambiguously coinciding with specified type of the winding. In case of tooth windings the amount of slots per pole and phase results a number lower than one. For the purpose of deeper analyses of tooth winding properties four types of them have been chosen, with amount of slots expressed as basic rational number: q = 1/4, 2/5, 3/8 and 1/2.

II. Analyses of Tooth Winding Properties

A. Winding Factor

The basic properties of tooth windings may be presumably obtained using traditional analytic methods, but for obtaining possibly most accurate results it is suitable to combine more different approaches for calculation of one parameter. E.g. the winding factor may be obtained as a product of the winding distribution factor and winding pitch factor as well as a result of calculation from Tingley schema of winding coil sides. This, as well as the winding phasor star, carries the information about the winding factor.

The traditional method mentioned in e.g. [4] introduces two separate winding properties – winding distribution factor and winding pitch factor – whose product is the final winding factor. The winding distribution factor (expressed generally for any ν-th harmonic component) is defined as

$$k_{dv} = \frac{\sin\left(v\frac{\pi}{2m}\right)}{q_0 \sin\left(v\frac{\pi}{2mq_0}\right)}, \tag{1}$$

where ν is the harmonic component order
m is the amount of winding phases
and q_0 is the numerator of q.

The numerator of amount of slots per pole and phase q_0 in (1) results from the definition of the amount of slots per pole and phase whose result is set to basic rational form:

$$q = \frac{q_0}{n} = \frac{Q}{2pm}, \tag{2}$$

where Q is the amount of winding slots
2p is the amount of poles
and n is the denominator of q.

As mentioned in Section I, the winding coil pitch of a tooth wining is set to one, without considering any relation to the machine pole pitch. This fact influences machine winding pitch factor, which is defined as

$$k_{pv} = \sin\left(v \frac{y_{1s}}{t_p} \cdot \frac{\pi}{2} \right), \quad (3)$$

where y_{1s} is the winding coil pitch
and t_p is the amount of slots per pole (pole pitch)

The equation (3) may be also simplified using known winding coil pitch $y_{1s} = 1$ to

$$k_{pv} = \sin\left(v \frac{\pi}{2t_p} \right), \quad (4)$$

where $2t_p$ may be also interpreted as amount of slots per machine pole-pair, thus a constant for a winding with specific amount of slots per pole and phase. Using (2) the amount of slots per machine pole-pair may be replaced by

$$2t_p = \frac{Q}{p} = \frac{2pmq}{p} = 2mq . \quad (5)$$

Considering (5) the winding pitch factor of a tooth winding results

$$k_{pv} = \sin\left(\frac{v\pi}{2mq} \right). \quad (6)$$

This proves that the tooth winding factor depends only on the amount of machine power supply phases and the winding amount of slots per pole and phase. Using the derived winding distribution and winding pitch factors the winding factor results

$$k_{wv} = k_{dv} k_{pv} . \quad (7)$$

This approach may be checked using calculation of the winding factor by the Tingley schema. The Tingley schema is formed by a table where each filled up field coincides with one phasor of the winding phasor star. In the schema axis of each phase may be found and used for calculation of the winding factor as

$$k_{wv} = \frac{\sum_n N_i \cos v\varphi_i}{\sum_n N_i}, \quad (8)$$

where

- i are the indices of columns belonging to one phase in the Tingley schema
- N_i is the amount of filled-up fields in i-th column of the Tingley schema
- φ_i is the angular distance between i-th column and corresponding phase axis

and

- n is the total amount of filled up columns in one phase of the Tingley schema.

Results comparing calculation of the winding factor using (1), (6), (7) and (8) are shown in Table I. As seen from Table I both approaches provide identical results (except of sign of the result), therefore both of them are valid for further analyses of tooth windings.

TABLE I.
WINDING FACTORS OBTAINED USING DIFFERENT APPROACHES

q	k_{d1} (1)	k_{p1} (6)	k_{w1} (7)	k_{w1} (8)
1/2	1.000000	0.866025	0.866025	0.866025
1/4	1.000000	0.866025	0.866025	0.866025
2/5	0.965926	0.965926	0.933013	0.933013
3/8	0.959795	0.984808	0.945214	0.945214

B. Differential Leakage Flux Factor

Together with the winding factor, expressing more likely the effectiveness of the winding, the differential leakage flux factor may be obtained using known winding topology. The differential leakage flux factor clearly defines the amount of undesired harmonic components of the magnetic field generated by the winding because of its topology. Therefore this winding property may be considered rather as "winding quality factor."

The traditional method of the differential leakage flux factor calculation is based on the analysis of Görges diagram – a two dimensional interpretation of the stator magnetomotive force (MMF). In case of an ideal winding the Görges diagram would converge to a circle with radius

$$R = \frac{m}{\pi} q k_{w1} \sqrt{2} I_s , \quad (9)$$

where $\sqrt{2}I_s$ is the amplitude of the current sum in one machine slot.

The radius of Görges diagram also corresponds with the magnitude of the fundamental harmonic component of the rotary magnetic field MMF. As stated in (9), the magnitude of the fundamental harmonic component is proportional to the current in machine slots. This fact makes any result specific to each machine separately. For the propose of obtaining generally valid result it is suitable not to consider real units but per-unit system by defining $\sqrt{2}I_s$ equal to one. The radius of Görges diagram in per-unit system [p.u.] is then

$$r = \frac{m}{\pi} q k_{w1} . \quad (10)$$

Since the space of the machine air gap is an environment with magnetically linear properties, the magnetic energy density stored in the air gap may be defined as

$$w_{mg} = \frac{1}{2} B_\delta H_\delta , \quad (11)$$

where B_δ is the air gap magnetic flux density
and H_δ is the air gap magnetic field strength.

The relation (11) may be simplified using known permeability of the air μ_0, which determines the relation between magnetic field strength and flux density to

$$B_\delta = \mu H_\delta , \quad (12)$$

and it results

$$w_{mg} = \frac{1}{2} \mu_0 H_\delta^2 . \quad (13)$$

According (13) the density of the magnetic field energy is proportional to a square of the magnetic field strength. Similar relation may be also found between the magnetic field strength and the magnitude of air gap MMF (expressed e.g. using (9)). Thus, the air gap magnetic field density is proportional to the magnetic field strength and also is proportional to the Görges diagram radius:

$$w_{mg} \sim H_{\delta}^{2} \sim R^{2} . \tag{14}$$

As mentioned before, the ideal shape of the Görges diagram is a circle with radius equal to R. Real division of the winding into slots and phases and a finite amount of coils and coil groups change Görges diagram into a polygon. The magnetic energy of such polygon is then an average of magnetic energies defined by each vertex of the polygon. The total magnetic energy of a general Görges diagram is

$$w_{m} \sim \frac{1}{n}\sum_{n} R_{i}^{2} , \tag{15}$$

where

R_i is distance of each vertex from the centre of the polygon.

The comparison of the total magnetic energy density with the magnetic energy generated by the fundamental harmonic component defined in (9) only shows the increase of the magnetic energy in the air gap. Such increase is caused by other harmonic components and is expressed as

$$\tau_{dif} = \frac{w_{m} - w_{m1}}{w_{m1}} \sim \frac{\frac{1}{n}\sum_{n} R_{i}^{2} - R^{2}}{R^{2}} , \tag{16}$$

or in per-unit system

$$\tau_{dif} = \frac{\frac{1}{n}\sum_{n} r_{i}^{2} - r^{2}}{r^{2}} , \tag{17}$$

where

r_i are distances of each vertex from the centre of the polygon drawn in per-unit system

and

τ_{dif} is ration known as differential leakage flux coefficient.

As seen from (17) the expression for differential leakage flux is very similar to calculation of the total harmonic distortion (THD) ratio, while w_m symbolizes the total power (energy) of machine magnetic field and w_{m1} the power (energy) of magnetic field fundamental component.

The equality of both approaches may be proved using traditional method of THD calculation from spectrum of the winding MMF space displacement.

The space dependence of the winding MMF may be obtained using known topology of the winding. The result is then a step-curve which may change its value at each slot along the stator periphery. In case of an ideal winding the step curve would converge to a sinusoidal function with magnitude equal to R or r in per-unit system respectively.

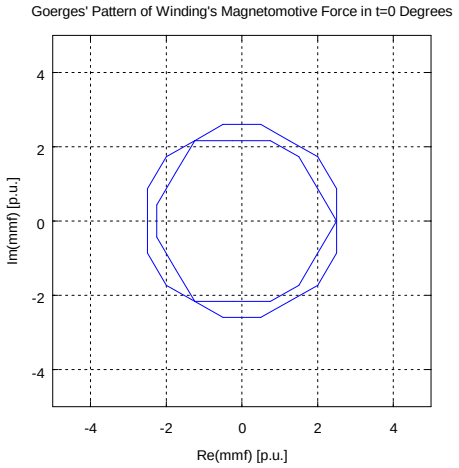

Fig. 2. Görges diagram of a distributed winding (q = 11/4).

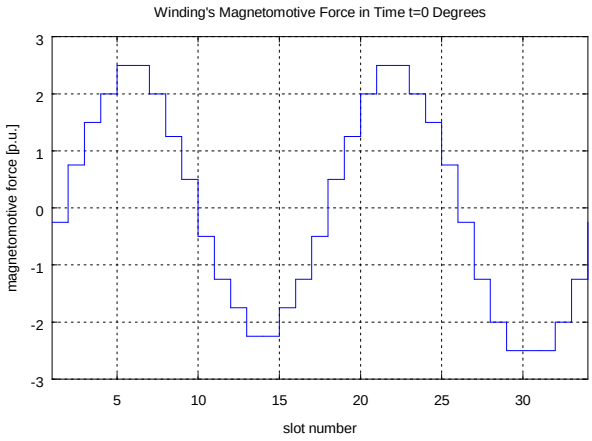

Fig. 3. Space dependence of distributed winding MMF (q = 11/4).

The magnitudes of harmonic components included in the magnetic field generated by the stator winding may be obtained via fast Fourier Transformation (FFT) and resulting total harmonic distortion (THD) [5] corresponds with differential leakage flux factor

$$THD = \tau_{dif} = \frac{\sum_{n} H_{i}^{2} - H_{1}^{2}}{H_{1}^{2}} = \frac{\sum_{2}^{n} H_{i}^{2}}{H_{1}^{2}} , \tag{18}$$

where

H_1 is the magnitude of fundamental harmonic component of the magnetic field strength

and

H_i is the magnetic field strength of i – th harmonic component.

The determination of the fundamental harmonic component H_1 used in (18) brings a contradiction between results of FFT and required value of H_1. Although the

results of FFT introduce H_1 as the first calculated harmonic component, the required value of the fundamental component of the magnetic field strength generated by the winding coincides with the wave length proportional to the amount of machine slots and the amount of its pole-pairs. Thus the wave length of the required fundamental harmonic component H_1 for usage in (18) is

$$\lambda_1 = \frac{Q}{p}. \tag{19}$$

As a consequence of this fact, the spectrum of the magnetic field in the air gap may include also sub-harmonic components. These sub-harmonic components have larger wave length than the fundamental harmonic component and also form a part of the magnetic field which does not produce usable torque and therefore these harmonic components have to be considered as harmonic components producing differential leakage flux.

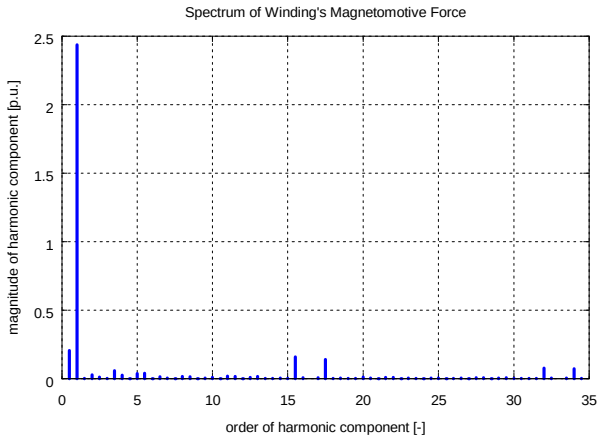

Fig. 4. Spectrum of MMF step-curve in Fig. 3 (q = 11/4).

The comparison of results of both approaches for calculation of the differential leakage flux is shown in Table II. As seen from the results both possibilities lead to very similar results. The excessive values of obtained results will be discussed in further sections.

TABLE II.
DIFFERENTIAL LEAKAGE FLUX COEFFICIENTS
OBTAINED USING DIFFERENT APPROACHES

q	τ_{dif} (17)	τ_{dif} (18)
1/2	0.462164	0.461818
1/4	4.848654	4.860046
2/5	0.968349	0.966946
3/8	1.182101	1.179694

III. THE AFTER-EFFECTS OF REAL MACHINE GEOMETRY

The after-effects of a real machine geometry and real material properties have been studied on a permanent magnet synchronous machine designed for the purpose of this research in four variants [6]. The nominal parameters of the machine are:

Nominal output power P_n = 60 000 W
Nominal speed n_n = 400 rpm
Amount of power supply phases m = 3
Amount of machine poles 2p = 40

The basic design considers q = 1/2 slot per pole and phase and it has been adopted for four variants mentioned in Section I. The winding has been considered as laid into opened slots, thus the effect of slot openings fully appears. The winding properties have been studied using programs FEMM [7] and Görges [8]. Since all studied properties also influence the machine torque and torque characteristic, these properties also have been studied using a Lua script [9] controlled FEMM calculation (see Section IV).

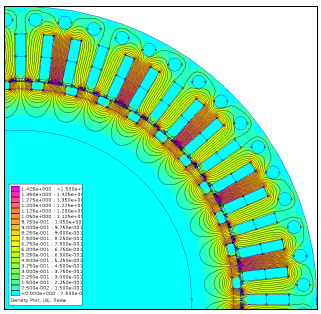

Fig. 5. Partial cross-section through designed machine

As mentioned before, the basic version of the designed machine considers one half of slot per pole and phase. This variant has been chosen because of very wide usage of this solution in the industry. It resulted in the design of stator with winding which has been placed in 60 slots. The theoretical winding MMF is shown in Fig. 6.

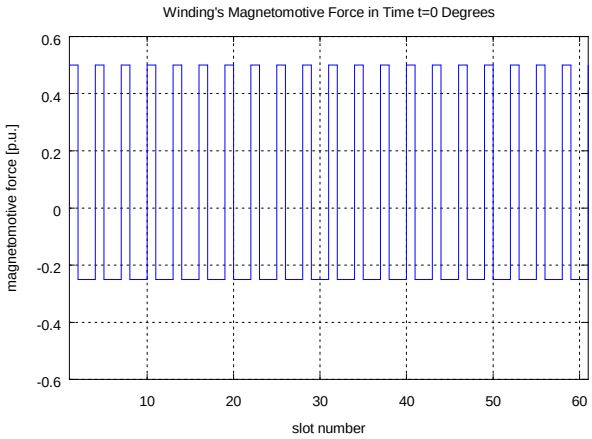

Fig. 6. Theoretical curve of MMF in machine air gap (q = 1/2).

The magnetomotive force along the machine stator is according to theory formed by a row of rectangles, which form together a 40-pole magnetic field. The rectangular progression of the magnetic field results in a high total harmonic distortion. In a real machine the space dependency of the MMF is influenced by saturation, slot openings and dissipation of the magnetic field.

The resulting curve (Fig. 7) therefore does not have as sharp edges and shows lowering of the magnetic field strength nearby the slot openings.

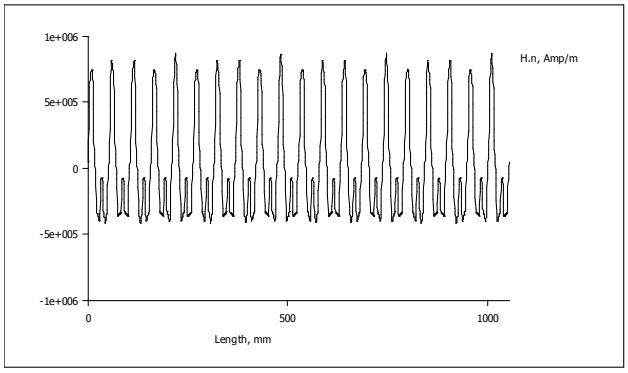

Fig. 7. MMF in machine air gap influenced by real geometry (q = 1/2).

The after-effect of real geometrical properties is lowering the amount of higher order harmonic components and their magnitude. The comparison of FFT of both MMF in Figs. 6 and 7 is shown in Figs. 8 and 9. In both FFT the fundamental harmonic component has the greatest magnitude followed by 2nd harmonic, which is in real geometry even higher than presumed.

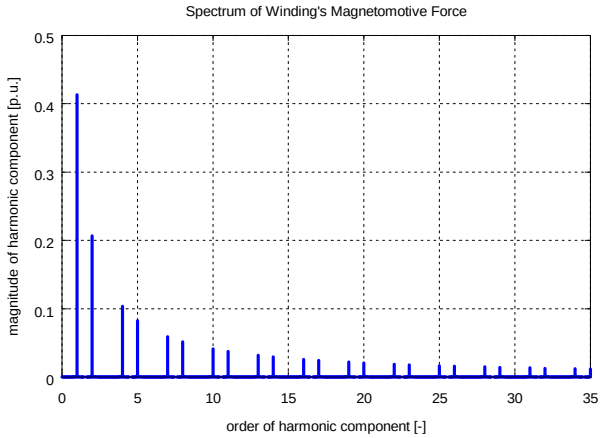

Fig. 8. Spectrum of theoretical MMF curve (q = 1/2).

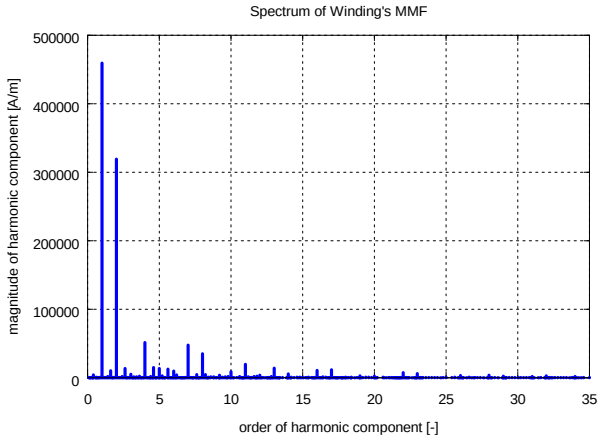

Fig. 9. Spectrum of MMF in machine air gap influenced by real geometry (q = 1/2).

Another point of view in this issue offers Görges diagram. Its traditional appearance near to a polygon with many vertices is in case of q = 1/2 winding simplified to a triangle. The difference of final Görges diagram from a circle also shows a possibility of high harmonic distortion of the magnetic field.

Second variant of the designed machine has been modified for q = 1/4 of slots per pole and phase, thus the resulting amount of the stator winding slots has been reduced to Q = 30. Such winding types are commonly used for brushless direct current machines (BLDC) and has been included mainly for comparison with q = 1/2 type winding. The resulting shape of the generated magnetomotive force by q = 1/4 winding is shown in Fig. 11.

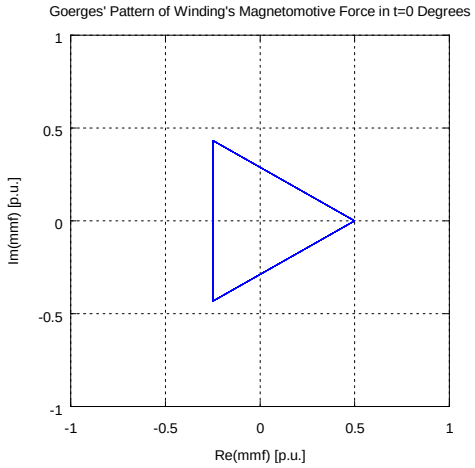

Fig. 10. Görges pattern of a winding with q = 1/2

The comparison of the MMF generated by q = 1/2 and q = 1/4 windings (Fig. 6 vs. Fig. 11) shows similarity of the generated MMF, but in case of q = 1/4 winding the MMF degenerates from 2p = 40 pole topology to only 2p = 20 poles. This fact should be expressed in FFT of the generated MMF by a considerable sub-harmonic component.

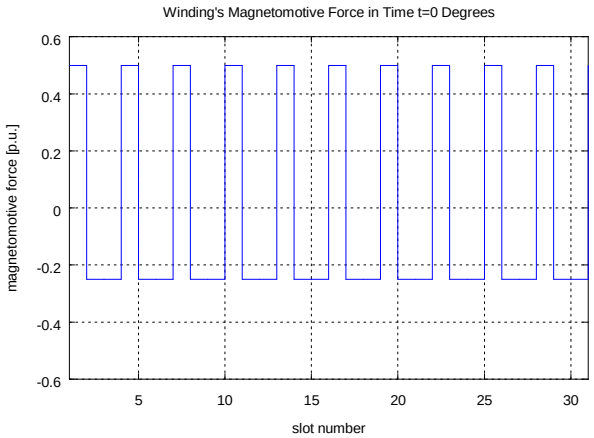

Fig. 11. Theoretical curve of MMF in machine air gap (q = 1/4).

The finite element analysis of the designed machine shows a significant influence by real geometry – previously mentioned effects areless visible thanks to slot openings. They again make the theoretically predicted curve less sharp and introduce further deformations of the magnetic field which result in additional harmonic components.

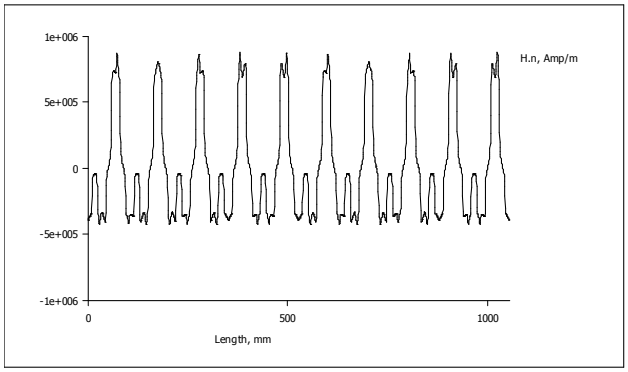

Fig. 12. MMF in machine air gap influenced by real geometry (q = 1/4).

The presence of the sub-harmonic component is confirmed by accomplished FFT of both previously mentioned MMF space dependencies (Figs. 13 and 14). Both spectres include significant "0,5th" harmonic component with greater magnitude than the expected fundamental harmonic component according to the design of the machine.

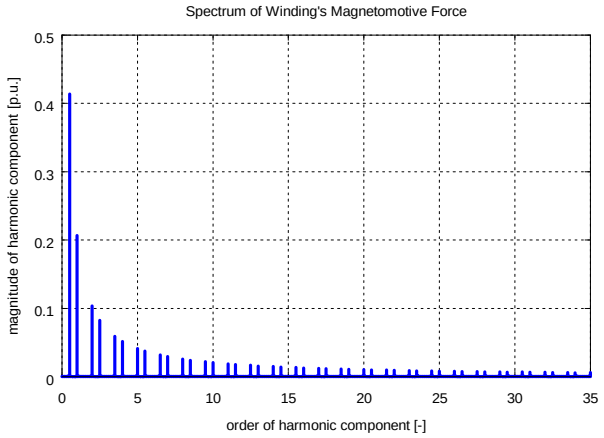

Fig. 13. Spectrum of theoretical MMF curve (q = 1/4).

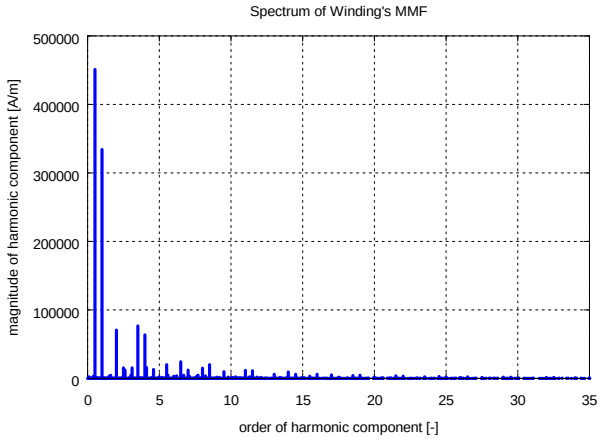

Fig. 14. Spectrum of MMF in machine air gap influenced by real geometry (q = 1/4).

The results of q = 1/2 and q = 1/4 show very similar after-effects of real geometry and non-linear physical properties of machine steel. The finite element analysis results do not include as high magnitudes of higher order harmonic components, but near to fundamental harmonic component a lot of "noise" produced by machine geometry exists.

In both versions of windings the second line in FFT has in case of real geometry higher magnitude than theoretically predicted. This effect reduces by q = 1/4 the distortion ratio, since in this case this is the fundamental harmonic component. In case of q = 1/2 winding this harmonic component may be considered as parasitic and therefore the effect on THD is antipodal.

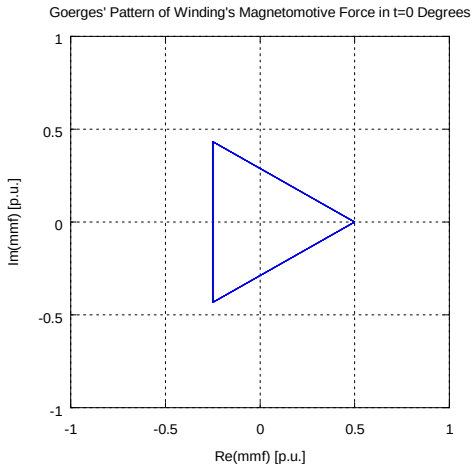

Fig. 15. Görges pattern of a winding with q = 1/4.

Third studied version of the machine utilized winding with q = 2/5 slots per pole and phase. The resulting magnetomotive force of the winding becomes in this case more complicated than in the previous versions. Theoretically predicted MMF space-dependence is shown in Fig. 16.

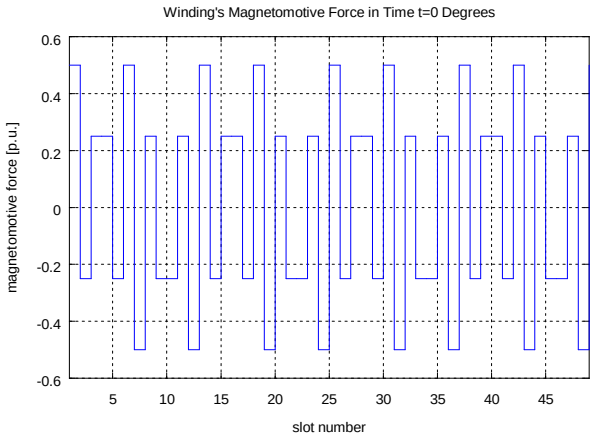

Fig. 16. Theoretical curve of MMF in machine air gap (q = 2/5).

The magnetomotive force space dependence of a q = 2/5 winding is not, in comparison to the previous cases, formed by a row of uniform rectangles. The pattern of these rectangles repeats after 10 machine poles.

The above mentioned repetition of the rectangular pattern consequently produces a sub-harmonic component of the magnetic field. Using FFT the order of this component results as "0.2nd," and it corresponds with 5 machine pole pair repetition of the magnetic field pattern.

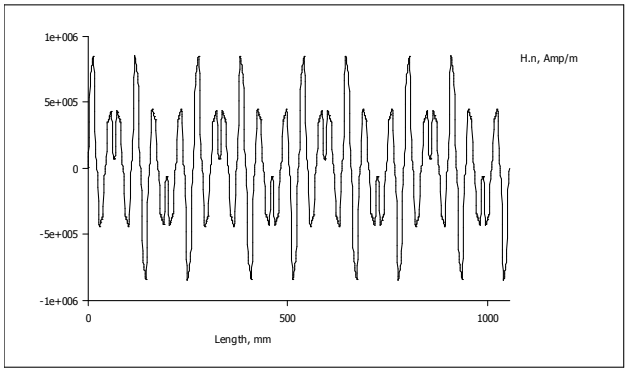

Fig. 17. MMF in machine air gap influenced by real geometry (q = 2/5).

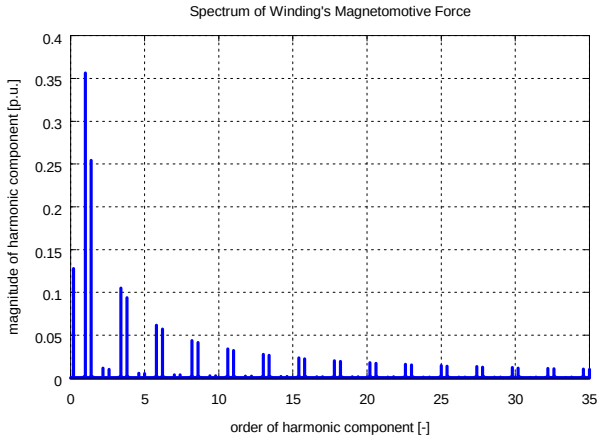

Fig. 18. Spectrum of the theoretical MMF curve (q = 2/5).

The comparison of spectres of theoretically predicted and FEM obtained MMFs confirms again suppression of higher order harmonic components and addition of "noise" near to the fundamental harmonic component. Similarly to the previous case a harmonic component following the fundamental harmonic component increases its magnitude in the FEM modelled machine.

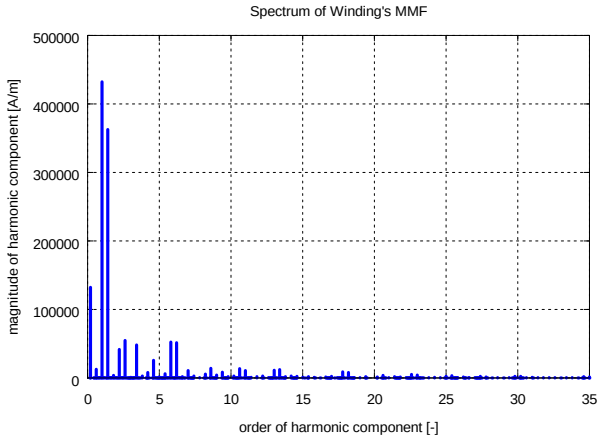

Fig. 19. Spectrum of MMF in machine air gap influenced by real geometry (q = 2/5).

The more complicated topology of the winding provides, except more complicated magnetomotive force space dependency, also more complicated shape of Görges pattern. In this case the Görges diagram results in superposition of two triangles with their axes.

Last solved case of the machine has been designed for winding with q = 3/8 slots per pole and phase. The behaviour of this winding type is very similar to the previous q = 3/8 type. Similarly to the previous type, the MMF also shows a repeating pattern with period equal to 8 machine poles, which also results in a sub-harmonic MMF component.

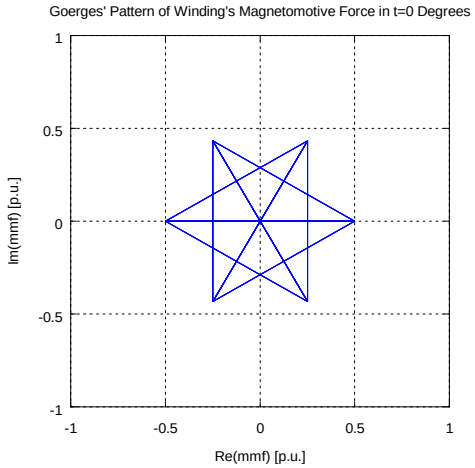

Fig. 20. Görges pattern of a winding with q = 2/5.

The theoretically predicted MMF space-dependence is shown in Fig. 21. In comparison to results obtained using FEMM (Fig. 22) the theoretically predicted step-curve again considers sharper edges of the generated MMF, than result from the FEM analysis.

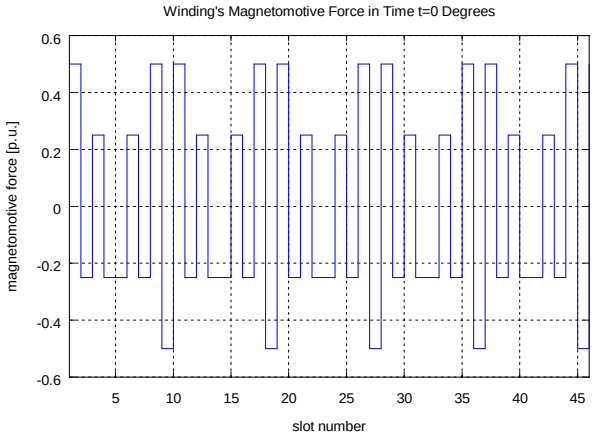

Fig. 21. Theoretical curve of MMF in machine air gap (q = 3/8).

The FFT analysis of both space dependencies approves presence of sub-harmonic component at 0.25 fold of the fundamental harmonic component. Together with this two more significant harmonic components appear at 0.5 and 1.25 fold of the fundamental harmonic component frequency.

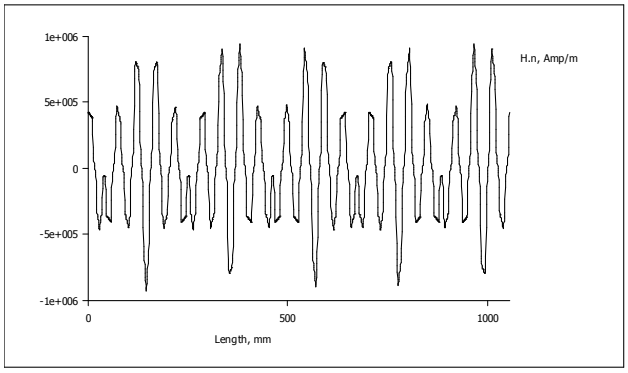

Fig. 22. MMF in machine air gap affected by real geometry (q = 3/8).

As seen from Figs. 23 and 24, the FEM results approve suppression of higher order harmonic components. Similarly to previous results the spectrum of FEM analysis includes more harmonic components with frequency near to the fundamental harmonic component.

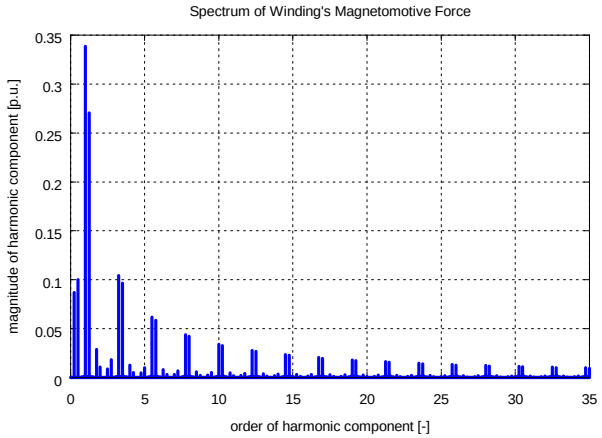

Fig. 23. Spectrum of theoretical MMF curve (q = 3/8).

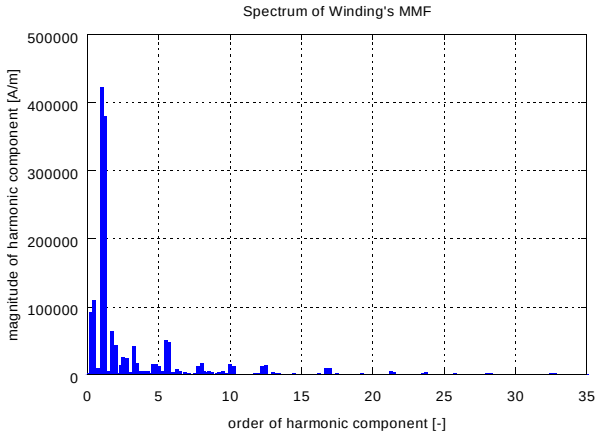

Fig. 24. Spectrum of MMF in machine air gap influenced by real geometry (q = 3/8).

A similarity with q = 2/5 winding may be also observed on obtained Görges pattern. The shape is very similar except one triangle missing in q = 2/5 winding Görges diagram. The resulting shape is therefore similar only to a triangle with extended axes.

Using relations (17) and (18) from Section II the differential leakage flux coefficients have been calculated for all studied winding types. The comparison of results obtained using Görges diagram (theoretical prediction) and from FFT of FEM model results is shown in Table III.

TABLE III.
COMPARISON OF THEORETICAL AND FEM RESULTS

q	τ_{dif} (theoretical)	τ_{dif} (using FEM)
1/2	0.46199	0.52170
1/4	4.85435	1.98970
2/5	0.96765	0.87349
3/8	1.18090	1.01970

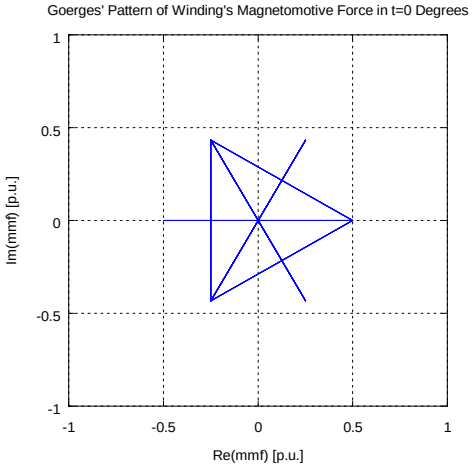

Fig. 25. Görges pattern of a winding with q = 3/8.

The results of the performed comparison show a good coincidence between theoretical prediction and results from FEM analyses. In most cases (except q = 1/2 winding) the real geometry of a machine with real physical properties leads to a decrease of the differential leakage flux coefficient and THD. According to the obtained winding properties the q = 1/4 winding is not suitable for usage on synchronous machinery because of presence of a high amount of harmonic components of different orders than the fundamental harmonic component.

IV. TORQUE PRODUCED BY THE MACHINE

The studied permanent magnet machine utilizes permanent magnets placed on the surface of the machine rotor, therefore from electromagnetic point of view this machine should have very similar properties to traditional synchronous machines with cylindrical rotor. For a synchronous machine with cylindrical rotor the torque characteristic is given by (neglecting stator winding resistance R_a) [10]

$$T = \frac{m}{\omega} \cdot \frac{V_t E_f}{X_s} \sin \beta , \tag{20}$$

where ω is the angular speed of machine rotation
V_t is the terminal voltage
E_f is the excitation voltage
X_s is machine synchronous reactance
and β is the torque angle.

Thus, the resulting torque characteristic of the designed machine should have sinusoidal shape with the amplitude:

$$T_{\max} = \frac{3}{41.89} \cdot \frac{240 \cdot 228}{1.89} = 2074.88 Nm\,, \qquad (21)$$

considering the terminal voltage V_t = 240 V, excitation voltage E_f = 228 V, synchronous reactance X_s = 1,89 Ω and nominal angular speed of the machine

$$\omega = \frac{\pi n}{30} = \frac{\pi \cdot 400}{30} = 41{,}89 rad \cdot s^{-1}\,, \qquad (22)$$

as these parameters result from machine design. The theoretical machine torque characteristic is shown in Fig. 26 and in further figures it is denoted by a dotted line for comparison with obtained FEM results.

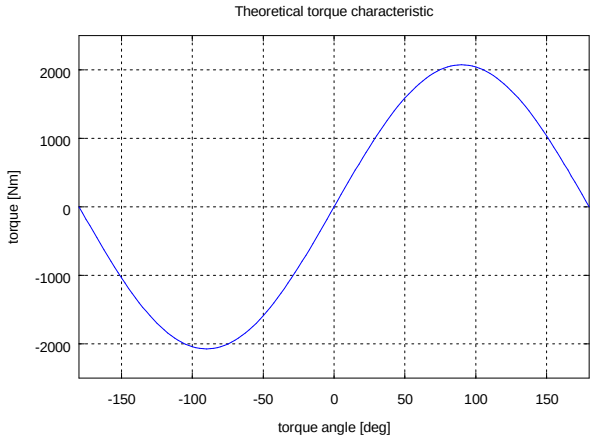

Fig. 26. Theoretical torque characteristic of the designed machine.

Fig. 27. Torque characteristic of machine with q = 1/2 winding.

The basic torque characteristic shown in Fig. 30 has been derived for presumption of sinusoidal magnetic fields of both stator and rotor, but in case of synchronous machine utilizing permanent magnets both magnetic field differ from ideal sinusoidal shape. Using program FEMM with embedded Lua scripting engine it is possible to examine the impact of the distorted stator magnetic field shown in Section III on the torque characteristic of the machine.

The basic designed version of the machine with q = 1/2 slots per pole and phase shows very high distortion of the basic torque characteristic. There are two significant torque saddles present in the machine characteristic, which lead to possibility of two torque angles for one requested value of torque. This property may worsen the control of the machine designed with this type of winding.

Second machine version with q = 1/4 of slots per pole and phase, shows similar behaviour like to the previous case, but one of the saddles disappears (transits only into corrugation of torque characteristic). Second torque saddle has lowered magnitude, but it also may lead to control instability. In this case a contrast between winding properties and torque properties appears. The q = 1/4 winding shows much worse properties than the q = 1/2 winding, but produced torque characteristic is better than in case of the q = 1/2 winding.

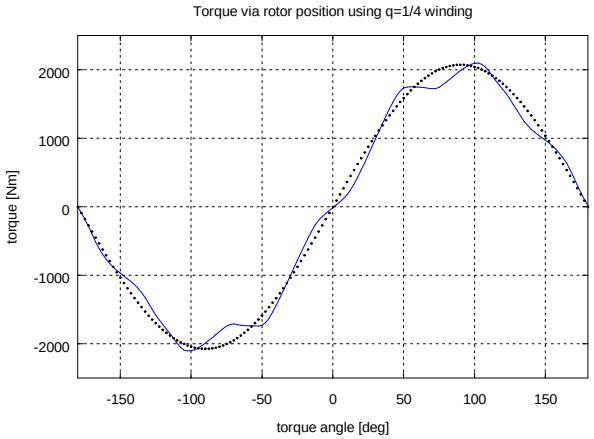

Fig. 28. Torque characteristic of machine with q = 1/4 winding.

Third studied case is focused on winding with q = 2/5 slots per pole and phase. In comparison to the previous cases all torque saddles disappear and the torque characteristic shows nearly sinusoidal behaviour. From this point of view the best results provides q = 3/8 winding, whose torque characteristic is almost purely sinusoidal.

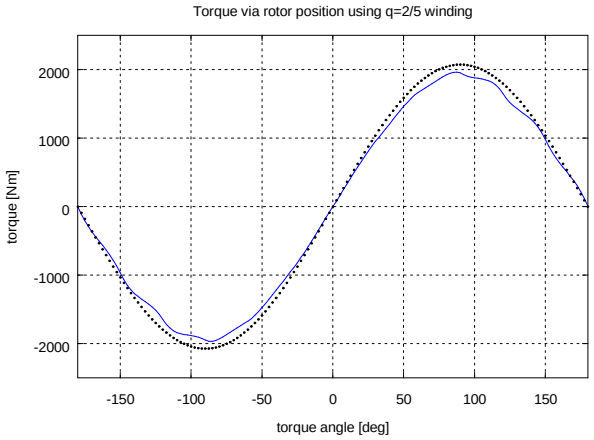

Fig. 29. Torque characteristic of machine with q = 2/5 winding.

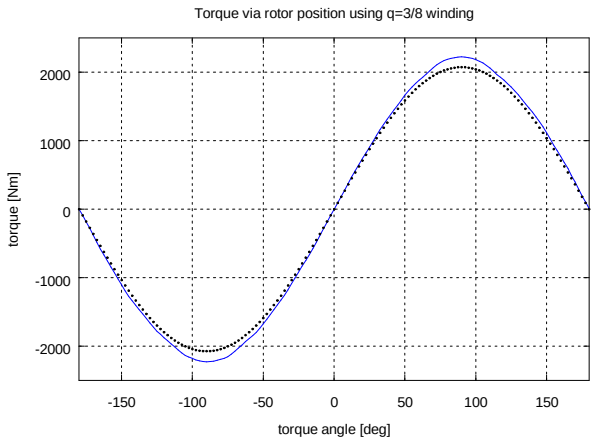

Fig. 30. Torque characteristic of machine with q = 3/8 winding.

V. Conclusion

In comparison to traditional windings the tooth windings introduce many harmonic components into the magnetomotive force of the stator winding. These harmonic components may be present in form of higher order harmonic components or sub-harmonic components. Since they do not produce utilizable torque, they are considered as one factor in the differential leakage flux coefficient.

According to theoretically obtained results, the differential leakage flux factor increases together with lowering of amount of slots per pole and phase. The lowest examined value applies to the q = 1/2 of slots per pole and phase winding and highest value to the q = 1/4 of slots per pole and phase. The after-effects of real geometry are more or less random. In case of the q = 1/2 winging the real geometry introduced additional harmonic components into MMF and therefore the differential leakage flux factor increased in comparison to theory. On the other hand in all other cases according to FEM analysis the real geometry decreased the real value of the differential leakage flux coefficient (see Fig. 31).

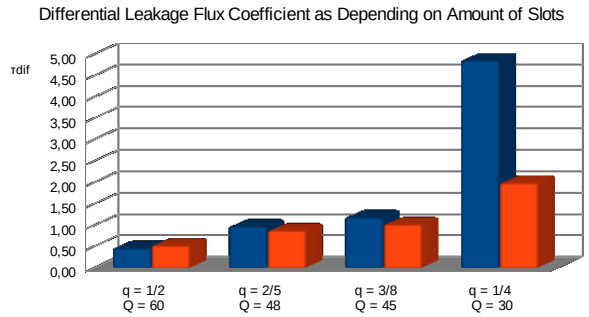

Fig. 31. Comparison of results for studied variants of tooth windings.

The torque produced by a machine utilizing tooth winding may be distorted as an after-effect of presence of high magnitude harmonic components in the stator MMF. For obtaining possibly smoothest torque characteristic it is suitable to choose more complicated winding topologies since simple winding topologies like q = 1/2 or q = 1/4 of slots per pole and phase introduce torque saddles into the characteristic. These torque saddles may lead to difficulties in control of the machine because of existence of more possible stable working points.

Acknowledgment

This research has been supported by the European Regional Development Fund and the Ministry of Education, Youth and Sports of the Czech Republic under the Regional Innovation Centre for Electrical Engineering (RICE), project no. CZ.1.05/2.1.00/03.0094.

References

[1] P. Salminen, "Fractional slot permanent magnet synchronous motors for low speed applications," *Dissertation, Lappeenranta University of Technology*, 2004.

[2] G. Müller , K. Vogt, B. Ponick, "Calculations of electric machinery (Berechnung elektrischer Maschinen)," *Wiley-Vch, Weinhein, Germany*, 2007. ISBN 978-3527405251

[3] Phase Motion Control Ningbo LTD, "Stator coil winding," [online] http://www.phasemotorparts.com/showing_149_149/stator-coil-winding.html, 2012. [Accessed: 7 Jan. 2013]

[4] J. Kučera, J. Hapl, "Winding of rotary electrical machines (Vinutí elektrických strojů točivých)." *ČSAV, Prague, Czechoslovak Republic*, 1959.

[5] L. M. Tolbert, H. D. Hollis and P. S. Hale, Jr., "Survey of harmonics measurements in electrical distribution systems," *IEEE IAS Annual Meeting, Oct. 6-10*, San Diego, CA, pp. 2333-2339, 1996.

[6] M. Sokol, "Design of permanent magnet synchronous machine (Návrh synchronního stroje s permanentními magnety)." *Master Thesis, UWB, Pilsen, Czech Republic*, 2012.

[7] D. C. Meeker, "Finite element method magnetics, version 4.0.1 (02Apr2007 Build)," [online] http://www.femm.info [Accessed: 10 Jan. 2013]

[8] K. Hruška, "Görges, version 1.51," [online] http://partnerstvi.fel.zcu.cz/vysledky/, 2012. [Accessed: 10 Jan. 2013]

[9] R. Ierusalimschy, L. H. de Figueiredo and W. Celes, "The Programming Language Lua," [online] http://www.lua.org [Accessed: 18 Jan. 2013]

[10] M.S. Sarma, "Electric machines: Steady-state theory and dynamic performance (second edition)." *West Publishing Company, St. Paul, USA*, 1997. ISBN-13: 978-0534938437